Biophysical Journal
Article

Biophysical Society

Quantifying Platelet Margination in Diabetic Blood Flow

Hung-Yu Chang,[1] Alireza Yazdani,[1] Xuejin Li,[1] Konstantinos A. A. Douglas,[2,3] Christos S. Mantzoros,[3] and George Em Karniadakis[1,*]

[1]Division of Applied Mathematics, Brown University, Providence, Rhode Island; [2]S. Lepida Biomedical Laboratory, Athens, Greece; and [3]Division of Endocrinology, Diabetes and Metabolism, Beth Israel Deaconess Medical Center, Harvard Medical School, Boston, Massachusetts

ABSTRACT Patients with type 2 diabetes mellitus (T2DM) develop thrombotic abnormalities strongly associated with cardiovascular diseases. In addition to the changes of numerous coagulation factors such as elevated levels of thrombin and fibrinogen, the abnormal rheological effects of red blood cells (RBCs) and platelets flowing in blood are crucial in platelet adhesion and thrombus formation in T2DM. An important process contributing to the latter is the platelet margination. We employ the dissipative particle dynamics method to seamlessly model cells, plasma, and vessel walls. We perform a systematic study on RBC and platelet transport in cylindrical vessels by considering different cell shapes, sizes, and RBC deformabilities in healthy and T2DM blood, as well as variable flowrates and hematocrit. In particular, we use cellular-level RBC and platelet models with parameters derived from patient-specific data and present a sensitivity study. We find T2DM RBCs, which are less deformable compared to normal RBCs, lower the transport of platelets toward the vessel walls, whereas platelets with higher mean volume (often observed in T2DM) lead to enhanced margination. Furthermore, increasing the flowrate or hematocrit enhances platelet margination. We also investigated the effect of platelet shape and observed a nonmonotonic variation with the highest near-wall concentration corresponding to platelets with a moderate aspect ratio of 0.38. We examine the role of white blood cells (WBCs), whose count is increased notably in T2DM patients. We find that WBC rolling or WBC adhesion tends to decrease platelet margination due to hydrodynamic effects. To the best of our knowledge, such simulations of blood including all blood cells have not been performed before, and our quantitative findings can help separate the effects of hydrodynamic interactions from adhesive interactions and potentially shed light on the associated pathological processes in T2DM such as increased inflammatory response, platelet activation and adhesion, and ultimately thrombus formation.

INTRODUCTION

Patients with type 2 diabetes mellitus (T2DM) are at high risk of developing cardiovascular diseases because T2DM is clearly linked with the onset of a thrombotic event (1,2). Several factors contribute to the prothrombotic status in T2DM, such as elevated coagulation, impaired fibrinolysis, endothelial dysfunction, and platelet hyperreactivity (3–5). Among them, the role of platelets in the formation and development of thrombi is of particular importance. Platelets in T2DM are characterized by dysregulation of several signaling pathways, and they can become hyperreactive and more prone to undesirable activation, adhesion, and aggregation (6–9). Other abnormalities such as raised platelet count and high mean platelet volume (MPV) have also been observed in T2DM (10,11). Shilpi et al. (12) showed that MPV (11.3 ± 1.0 fL) in diabetics is significantly higher than the MPV (9.0 ± 0.6 fL) in nondiabetics. For diabetic patients with micro- or macrovascular complications, MPV can be even higher (13,14). Papanas et al. (13) found that T2DM patients without retinopathy have an MPV = 10.9 ± 1.1 fL, whereas those with retinopathy have an MPV = 15.8 ± 1.3 fL. It is reported that large platelets are more reactive than smaller platelets (15), produce more prothrombotic factors such as thromboxane A2, and express a greater number of adhesion receptors, such as P-selectin and GpIIb/IIIa (16).

The process of thrombus formation and development at an injured site on a blood vessel wall involves a number of simultaneous processes from flow dynamics, blood coagulation cascade, and transport of tissue factors to platelet adhesion, activation, and aggregation (17–19). Thrombosis

Submitted June 12, 2018, and accepted for publication August 24, 2018.

*Correspondence: george_karniadakis@brown.edu

Hung-Yu Chang and Alireza Yazdani contributed equally to this work.

Editor: Mark Alber.

https://doi.org/10.1016/j.bpj.2018.08.031

can occur in the arterial or the venous circulation, and it is triggered by a disruption in endothelial cells and the exposure of tissue factors and collagen to blood. Accelerated atherosclerosis observed in T2DM would increase the risk of endothelial erosion of plaques, followed by thrombus formation (20). For efficient adhesion to an injured site, platelets must be sufficiently close to the site for platelet-subendothelium or platelet-platelet bonds to form. In a shear flow, red blood cells (RBCs) experience a wall-normal force that arises because of their deformation and propels them away from the vessel wall, leading to the formation of a cell-rich region in the core of the vessel and a cell-free layer (CFL) near the wall (21–23). This phenomenon was first quantified by Fahraeus and Lindqvist (24). Deformable RBCs, on the other hand, can expel platelets from the core of the stream toward the CFL region. Such transport and accumulation of platelets near the wall known as platelet margination occurs in the presence of RBCs at sufficient hematocrit (H_{ct}) and flowrate.

Significant progress has been made in understanding the platelet margination probability and dynamics, which characterize the physical contacts of platelet with the vessel wall and its direct or indirect effects on platelet adhesion. The first in vivo experiments of platelet distribution in venules and arterioles of rabbit mesentery were performed by the group of Reneman et al. (25–27). They found that the normalized platelet density is concentrated near the wall of arterioles, but the opposite platelet distribution is observed in venules. This discrepancy may be due to the rheological effects of RBCs, different position of a vessel in the vascular network, and also vessel wall properties. Numerous in vitro studies on the platelet margination and adhesion have also been reported (28,29). Aarts et al. (30) examined the radial distribution of RBCs and platelets in 3-mm cylindrical vessels at various hematocrit and wall shear rates by the laser-Doppler technique. They found that near-wall concentration of platelets increases with increasing hematocrit and wall shear rates. Similar results of enhanced margination of platelet-sized spherical particles for $H_{ct} = 20\%$ compared to $H_{ct} = 10\%$ were found by Fitzgibbon et al. (31). In addition to the experiments, they conducted boundary integral simulations to confirm their experimental results and to track the trajectories of the particles with higher resolution. Eckstein and co-workers (32,33) performed several studies on the lateral transport of platelet-sized latex beads in flows of blood suspensions. They found that the near-wall excess in concentrations of platelet-sized beads occurred when $H_{ct} > 10\%$ and the wall shear rate $> 200\ s^{-1}$, whereas the largest amount of lateral transport of beads was observed at moderate shear rate $\sim 560\ s^{-1}$.

Along with the aforementioned experimental studies, recent advances in computational modeling and simulations enable us to investigate blood flow dynamics under physiological and pathological conditions (34–38). Crowl and Fogelson (39,40) have performed blood flow simulations in a two-dimensional channel using a Lattice Boltzmann Method. They found that the lateral diffusivity of a platelet is correlated with its lateral position and platelet margination mostly occurs after the CFL has fully developed. The numerical studies from the group of Aidun et al. (41–43) demonstrated that, in addition to the hematocrit, the viscosity ratio of cytoplasm within the RBC to suspending fluid as well as the platelet shape play an important role in the margination process; less viscous cytoplasm of RBC than plasma or a more spherical shape of platelets can enhance the platelet margination rate. Vahidkhah et al. (44) have captured the three-dimensional nature of RBC-platelet collisions. For platelets approaching the wall, anisotropic platelet diffusion within CFL leads to the formation of platelet clusters, which might contribute to clot formation. Soares et al. (45) and Yazdani and Karniadakis (46) have performed simulations of platelet transport in complex geometries resembling arterial stenoses. They employed dissipative particle dynamics (DPD) to investigate the transport dynamics and self-orbiting motions of platelets when they flow through a constriction. Yazdani and Karniadakis (46) also found that higher levels of constriction and wall shear rates enhance platelet margination significantly, which may consequently lead to enhanced poststenosis platelet deposition onto the thrombus. In addition, the effects of microvessel tortuosity and the pathological alteration in the platelet size and density on the platelet activation and thrombus formation have been systematically investigated by Chesnutt and Han (47). In their study, however, they considered platelets as spherical particles and neglected the effects of RBCs for computational efficiency.

Following our previous work on modeling diabetic RBCs (48), here we extend our simulations to complex blood flow in microcirculation to study correlations between T2DM and increased platelet margination. We perform high-fidelity computational studies of blood flow through cylindrical vessels and focus on the radial distribution of diabetic RBCs and platelets under conditions resembling blood flow in an arteriole for T2DM subjects. In particular, we incorporate the properties of diabetic RBCs and platelets from available experiments and also a new data set collected from 64 diabetic patients. Several hemodynamic factors such as blood flowrate, hematocrit, and platelet shape are taken into account. In addition, there is growing evidence showing that white blood cells (WBCs) contribute to the disturbances of microcirculation in diabetes because of the promoted inflammatory cell recruitment (49–51). We further consider the influence of WBC dynamics on platelet transport in blood vessels by respectively incorporating leukocyte circulation, rolling along the vessel wall, and firm adhesion to the wall into our simulations. Such in silico hematologic studies involving large population of blood cells enables us to gain insights in the circulation and distribution of RBCs, platelets, and leukocytes in diabetic conditions, which in turn

will help us understand the connection between enhanced thrombosis and inflammation in T2DM (52).

METHODS

We employ DPD to model whole blood flow, i.e., plasma, RBCs, platelets, and WBCs, in 40-μm diameter vessels. DPD is a coarse-grained analog of molecular dynamics in which each particle represents a lump of molecules that interacts with other particles through soft pairwise forces. In addition to blood plasma modeled by collections of free DPD particles, the membrane of suspending cells including RBCs, platelets, and WBCs is constructed by a two-dimensional triangulated network with N_v vertices (DPD particles).These vertices are connected by N_s elastic bonds to impose proper membrane mechanics. More details of hydrodynamic interactions between DPD particles, and models for blood cells are presented in the Supporting Materials and Methods. We also validated systematically the DPD model by simulating the margination of spherical particles of different sizes in blood flow and compared against recent microfluidic measurements (53). The validation results are given in the Supporting Materials and Methods.

Parameter estimation

RBC models

Under physiological conditions, a healthy RBC has a large area/volume (S/V) ratio with a biconcave shape and a remarkable deformability and adaptability in mechanical behavior. In this study, we model an RBC at normal state (NRBC) with $N_v = 500$, shear modulus $\mu_0 = 4.73$ μN/m, and bending rigidity $k_0 = 2.4 \times 10^{-19}$ J. An NRBC is set to have the cell surface area $A_0^{tot} = 132.9$ μm^2 and cell volume $V_0^{tot} = 92.5$ μm^3, which give $S/V = 1.44$. All parameters used in our NRBC model are extracted from available measured data, and the representative RBC model has been extensively used from single-cell mechanics to blood flow dynamics (22,23,54,55). Different from NRBCs, diabetic RBCs possess decreased cell deformability and are known to exhibit shape change from a normal biconcave shape to a near-oblate shape with a smaller S/V ratio (9,56,57). In addition, it was observed that the increase in mean corpuscular volume (MCV) is related to high blood glucose level (58,59). Diabetic RBCs with high intracellular glucose will induce osmotic imbalance between RBCs and their surrounding plasma. Morse et al. have shown an increase in MCV from 93 to 114 μm^3 by in vitro incubation of normal RBCs with glucose concentration of 20 mg/mL for an hour. A further increase in MCV (>120 μm^3) can be achieved with increasing incubation temperature (59). This MCV change is reversible once the glucose concentration is diluted. Agrawal et al. also claimed that the swollen RBCs observed from the sample blood of T2DM patients can be associated with the possible metabolic disturbance (60).

In this work, we have performed an evaluation of several clinical characteristics in blood samples from 136 human subjects (see Table S4). The number of patients diagnosed with T2DM is 64 with a mean age of 61 $\pm$ 13.7 years, compared to 72 patients with a mean age of 52 $\pm$ 17.8 years in controls. The blood glucose parameters, hemoglobin A1c (HbA1c), and fasting blood glucose (FBG) are significantly higher in diabetics (HbA1c = 7.66 $\pm$ 1.41% and FBG = 144.5 $\pm$ 48.9 mg/dL) compared to the controls (HbA1c = 5.25 $\pm$ 0.29% and FBG = 99.0 $\pm$ 15.4 mg/dL). Details of the blood sample preparation and analysis procedures are included in the Supporting Materials and Methods. As shown in Fig. S3, a and b, diabetic RBCs exhibit no statistically different MCV compared to that of the normal RBCs. A recent study performed by Lee et al. (61) shows a reduction in the membrane fluctuation of diabetic red cells, but there was no statistical difference in volume and surface area distributions of nondiabetic and diabetic RBCs. Although the alteration in the size and shape of diabetic RBCs is still debatable and probably dependent on glycemic control of the study subjects, we considered extreme values for S/V that were reported by Jin et al. (57). We have recently proposed a T2DM RBC model (48), which has been validated with available experimental data. Following our previous study, here, we extend our T2DM RBC model (DRBC) to a suspension with cell properties similar to those of a NRBC except for a shear modulus $\mu_s = 2\mu_0$ (μ_0 is the shear modulus of healthy subjects) and a reduced S/V ratio, $S/V = 1.04$.

Platelet models

An inactivated platelet is an oblate spheroid that can be characterized by its aspect ratio (AR) defined as the ratio of the minor axis to major axis. The typical AR range for a normal platelet is 0.25–0.5, and the MPV is 6–10 fL (μm^3) (62,63). However, previous studies have revealed a higher MPV in diabetic patients than in nondiabetic controls, which is considered as a risk factor for vascular diseases (12). As shown in our statistical study in Fig. S3, c and d, the scattered data points and the number distribution of MPV are significantly higher in the diabetic group than in the control group. The average MPV in diabetic subjects is 10.0 $\pm$ 1.26 fL compared to 9.2 $\pm$ 1.70 fL in nondiabetics, with a p-value of 0.003. Such enhancement in the MPV of diabetic platelets may be due to osmotic swelling as a result of hyperglycemia. Patients with less well-controlled diabetes are the ones developing micro- and macrovascular complications such as retinopathy. In a previous study by Papanas et al. (13), diabetic patients with retinopathy had an MPV = 15.8 $\pm$ 1.3 fL, which corresponds to a ~5 fL difference between the MPV (10.9 $\pm$ 1.1 fL) of diabetics without retinopathy. In addition to diabetic retinopathy, large databases with different categorizations (a wide range of HbA1c levels, other complications of diabetes, smoking history, age, gender, etc.) are needed to calibrate the current MPV values. Indeed, levels of glycemic control could have significant implications because the effect observed here could be much more pronounced in diabetics with poor glycemic control, who by definition are at much higher risk for developing cardiovascular disease (CVD) (1). Another potential factor is smoking, which has vasoconstrictive effects and is known to have multiplicative effects in terms of increasing CVD risk among diabetics (64).

Considering these facts, here, we started our efforts in this field by using the platelet model with cell volume based on patient-specific data and further conduct a sensitivity study. A normal platelet (PLT) has cell volume $V_0^{tot} = 6$ μm^3, whereas a diabetic platelet (PLT*) has $V_0^{tot} = 12$ μm^3. These extreme values are chosen to distinguish the platelet margination in diabetic blood from that in normal blood. In addition, we assume that the platelets are not activated, and they are modeled in an oblate-spheroid shape with the AR = 0.38. The major axis for PLT is 3.3 μm, whereas for PLT*, it is 4.1 μm. The number of vertices in membrane network $N_v = 48$ and elastic properties of platelets $\mu_s = 100$ μ_0 and $k_c = 16$ k_0 are given to all platelet models. Note that platelets are considered nondeformable in their resting state; however, they exhibit mild deformation with no activation under moderate shear rates (65,66). In this study, the elastic properties of platelets are given based on the fact that platelets are about one to two orders of magnitude stiffer than RBCs (65,67,68), and we keep μ_s and k_c parameters constant in all simulations. Platelet models with such high values of shear modulus and bending rigidity have also been extensively used to the study of platelet dynamics (39,44,46,69,70).

WBC model

A WBC is represented as a triangulated sphere with $N_v = 2498$ and a diameter of 10 μm, which is similar to the previous leukocyte model used by Lei and Karniadakis (71). Compared with healthy RBCs, a WBC is less deformable, with the estimated membrane stiffness 0.3–1.2 dyn/cm (72). It is also reported that impaired deformability has been observed in children with diabetes (73), but the changes in WBCs shape are unclear. In this study, we model a WBC with a membrane elasticity of $\mu_s = 22$ μ_0 and $k_c = k_0$.

Fluid-cell, cell-cell, and fluid (cell)-wall interactions

Blood plasma is modeled by DPD fluid with viscosity $\eta = 1.25 \times 10^{-3}$ Pa $\cdot$ s. The fluid-cell interactions are accounted for through viscous

friction using the dissipative and random DPD forces (see Supporting Materials and Methods for details). Cell-cell adhesive interactions exist among cells and may be amplified in several pathological conditions (e.g., sickle cell anemia, malaria, and diabetes) (74). In this study, we neglect the complex surface features of all blood cells and do not model cell-cell adhesive interactions to study systematically the hydrodynamic interactions that induce platelet margination. As two cells approach each other, strong repulsive lubrication forces develop preventing cells from overlap. We use DPD particles for both plasma and cell membranes for which the conservative repulsive forces ($\mathbf{F}^C$) are not strong enough to prevent cells from contacting each other. Therefore, we adopt a Morse potential between cell membrane particles to ensure strong repulsive forces and prevent cell overlap. Only the repulsive part of the Morse potential is used for cell-cell interactions, for which the well depth parameter is adjusted appropriately to ensure enough clearance between the cells. Further, to simplify the representation of platelets and WBCs, we apply the same cell-cell interaction parameters for both platelets and WBCs. The parameters used for the fluid-cell and cell-cell interactions are given in Tables S1–S3 in the Supporting Materials and Methods. The adhesive interactions between different pairs of blood cells such as RBC-RBC and RBC-WBC can also be captured by proper tuning of a Morse potential model. Fedosov et al. (75) simulated RBCs aggregation and the formation of rouleaux structures by applying Morse potential interactions between RBCs. Similarly, Lei and Karniadakis (71) modeled the interactions between the adherent leukocytes and sickled RBCs by the Morse potential. Furthermore, the vessel wall is modeled by frozen DPD particles with the same radial distribution function as the fluid particles in combination with a specular reflection of the plasma and cell particles at the fluid-wall interface (22,23). The scaling of model and physical units is also presented in the Supporting Materials and Methods. In all simulations, the length scale $r^M = 1.0 \times 10^{-6}$ m and the timescale $\tau = 1.8 \times 10^{-4}$ s are adopted.

Simulation setup

The blood flow domain is a cylindrical vessel with diameter $D_t = 40$ μm and periodic in the flow direction, as shown in Fig. 1 *a*. NRBCs in their resting form are biconcave in shape, whereas DRBCs are near oblate in shape. PLTs and PLT*s are both in oblate spheroid shape with AR = 0.38, but a PLT* has a cell size twice the size of PLT. In this study, the volume fraction of RBCs, i.e., average hematocrit (H_{ct}), is varied, whereas the number of platelets in the blood is fixed at 437,000 platelets/mm^3 (128,000–462,000 platelets/mm^3 for normal blood (76)). All fluid particles and blood cells are randomly placed within the vessel for the initial condition. To drive the flow (simple fluid or blood) in the vessel, we apply a constant body force to each DPD particle in the flow direction. The simulations are performed for sufficient time to achieve steady state, which is characterized by a time-independent fully developed velocity profile, i.e., a plug-like profile for blood. In this study, the time to reach steady state is equal to approximately a half second in physical units. Fig. 1 *b* shows the time-averaged axial velocity distribution for the healthy blood at $H_{ct} = 15\%$. The data is fitted with a parabolic curve (*red line*) that follows a plug-like characteristic. This plug-like velocity profile is due to the nonuniform distribution of RBCs in the vessel. RBCs in Poiseuille flow migrate to the vessel center forming a depleted region, the CFL, at the periphery of a vessel. A sample snapshot of NRBCs concentrated in the core region and PLTs marginated toward the wall is shown in Fig. 1 *c*. To vary the flowrate, we define a characteristic shear rate $\dot{\gamma}_w = 4\overline{u}/R_t$, where $\overline{u}$ is the mean velocity and R_t is the vessel radius. $\dot{\gamma}_w$ corresponds to the wall shear rate of a parabolic Poiseuille flow with the same $\overline{u}$ and is varied in our simulations. In addition, the cell Reynolds number is defined based on $\dot{\gamma}_w$, RBC diameter (D_{RBC}), and the kinematic viscosity of plasma (ν), $\mathrm{Re}_{cell} = \dot{\gamma}_w D_{RBC}^2/\nu \approx 0.05$, which renders the inertia effect negligible.

Our clinical data as well as previous studies have shown increased WBC recruitment and count in blood circulation in T2DM (49–51). In diabetics, P-selectin and intercellular adhesion molecule-1, which play important roles in the adhesion of leukocytes to endothelium, are significantly elevated in human retina and choroid (77). In addition, the rise in WBC count has been observed in our blood samples from diabetic patients (8.04 ± 2.16 k/μL) compared to control subjects (6.85 ± 1.96 k/μL) (see Table S4). We use our computational framework to investigate three different states of WBC dynamics in blood vessels: circulating in the blood stream, rolling on the wall, and adhered to the wall. For the last two states, we assume that WBCs and endothelial cells are activated and there are adhesive interactions between the receptors of WBCs and the associated ligands expressed on the endothelial surface. Depending on the type and strength of adhesive interactions, WBCs could roll or adhere on the endothelial surface. At physiological shear rates, rolling with selectin molecules (e.g., P- and E-selectins) is a prerequisite for chemoattractant-stimulated interaction of WBC integrins with endothelium intercellular adhesion molecule-1 that arrests rolling WBCs and strengthens adhesion (77–79). To simulate WBC rolling behavior, we initially place WBCs close to the

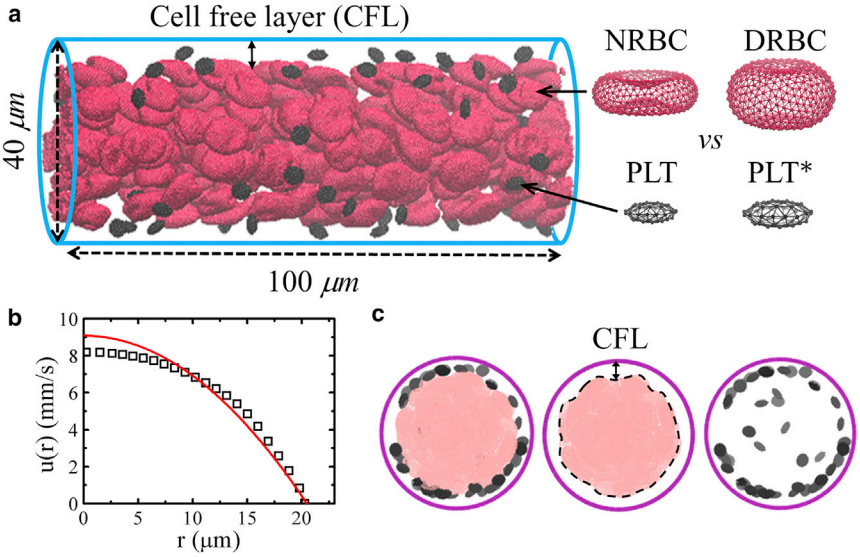

FIGURE 1 A typical simulation setup. (*a*) Side view of the healthy blood flow in a vessel with diameter $D_t = 40$ μm and hematocrit = 15%. The cell-free layer (CFL) is evident at fully developed blood flow, red cells are deformable NRBCs with biconcave shape in their resting form, and small black cells are PLTs. Diabetic blood in a vessel is composed of DRBCs with near-oblate shape in their resting form and larger in size PLT*s. (*b*) A plug-like velocity profile is achieved, and a parabolic curve (*red line*) is superimposed for reference. (*c*) Front views of the vessel. Snapshots from left to right show the distributions of red cells and platelets at steady state. To see this figure in color, go online.

wall and apply a weak conservative repulsive force between DPD particles of WBCs and the wall. To set up blood flow with adherent WBCs, we first run a short period of simulation with rolling WBCs, then freeze those DPD particles located at the interface between WBCs and the wall.

RESULTS AND DISCUSSION

Having validated our cell transport model with in vitro experiments (53) in the Supporting Materials and Methods, here, we first present the results of healthy blood flow in a vessel and make comparisons with other numerical and experimental studies for further validation. We then study blood flow in diabetic conditions using a suspension of DRBCs and T2DM platelets with a higher MPV value (PLT*s). The time-averaged concentration profiles of modeled RBCs and platelets flowing through vessels are plotted for different flowrate and hematocrit values. In addition, we investigate the shape effects of platelets on their transport. Subsequently, we take into account the WBCs by including their different dynamics in our flow simulations and analyze their contributions to platelet dynamics and transport.

Flow of healthy and diabetic blood

Fig. 2 shows the local concentration profiles of platelets and RBCs in the vessel ($D_t = 40\ \mu$m). Here, blood is in two states, i.e., healthy or diabetic, while the wall shear rate and average hematocrit are kept fixed at $\dot{\gamma}_w = 1000\ s^{-1}$ and $H_{ct} = 20\%$, respectively. Note that this flow condition is set based on the fact that platelets have higher near-wall presence in arterioles than in venules (27) and the mean hematocrit $H_{ct} = 16$–20% is a physiologically relevant value in small vessels (31,80,81). All simulations are performed for at least 3000 DPD time units (~0.54 s) to achieve steady flow conditions, and the last 500 time units are used for the estimation of the time-averaged concentration of RBCs and platelets. These time-averaged concentration profiles are also spatially averaged along the flow direction and plotted against the radial distance from the wall. A histogram bin in the platelet concentration profile represents the number of platelets within a cylindrical shell with volume V_j (platelets/μm^3) having a thickness of 0.5 μm. A cylindrical shell j has volume $V_j = \pi(r_o^2 - r_i^2) \times L$, where r_o is the outer radius, r_i is the inner radius, and L is the length of the shell, e.g., $V_{j=5} \approx 5576\ \mu m^3$ at $r_o = 18.0\ \mu$m, $r_i = 17.5\ \mu$m, and $L = 100\ \mu$m. If the average number of platelets in the shell $j = 5$ is 20, then the cell-center density of platelets within the shell $j = 5$ is ~0.36% (platelets/μm^3). The local RBC concentration profile is the cell-center density distribution normalized with respect to the mean prescribed density in that shell (ρ_j). For example, we have 270 NRBCs, and hence $\rho_j = 270 \times V_j/V_t$, where V_t is the total volume of the cylindrical vessel; similarly for DRBCs, for which we have 200 cells due to their larger size. Therefore, this normalized RBC distribution is adopted to eliminate the cell number difference between the modeled NRBCs and DRBCs.

In healthy blood flow, the distribution of NRBCs is increased around the center of the vessel, exhibiting a primary peak at the centerline and a secondary peak just outside the cell-free region (Fig. 2 *a*). Similar RBC distributions were found in previous studies (22,23). A high cell density of NRBCs in the vessel center is due to the relatively small shear rate in that region, which allows a close packing

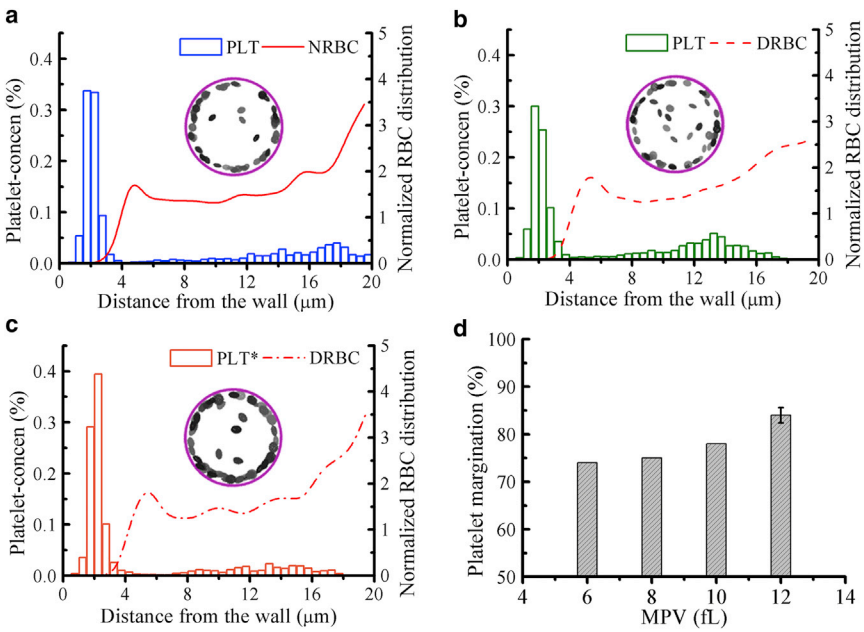

FIGURE 2 Difference in platelet margination between healthy and diabetic RBC + platelet suspensions. Concentration profiles of platelets and RBCs in the vessel for the cell suspensions of (*a*) NRBCs + PLTs, (*b*) DRBCs + PLTs, and (*c*) DRBCs + PLT*s. Snapshots showing the front views of vessels with platelets only at time = 0.54 s. (*d*) The percentage of platelet margination for platelets with different MPV values suspended in diabetic RBCs (DRBCs) and plasma. The vessel diameter $D_t = 40\ \mu$m, average hematocrit $H_{ct} = 20\%$, and wall shear rate $\dot{\gamma}_w = 1000\ s^{-1}$ remain the same for all cases. The error bar is obtained by performing three simulations with different random seeds to generate fluctuations in plasma and cell-cell interactions in the blood flow. To see this figure in color, go online.

of NRBCs. Away from the vessel center, the shear rate is increased, leading to the destruction of the close-packed structure of NRBCs. A peak in the distribution occurs next to the CFL, caused by the alignment of NRBCs and their cell centers that have similar radial positions. On the other hand, nondeformable PLTs are expelled by deformable NRBCs to the wall and dispersed in the CFL region. The formation of the CFL reduces the hydrodynamic resistance and also further promotes platelet margination. The CFL thickness can be determined by $\delta = R_t - R_{core}$, where R_{core} is the average radius of the center-occupied RBC core (see also a snapshot of RBC core shown in Fig. 1 *c*); $\delta \approx 2.75$ μm is estimated for the healthy blood, with $H_{ct} = 20\%$ flowing through a vessel with diameter = 40 μm, which is close to that obtained by Mehrabadi et al. (42) ($\delta = 3$ μm) for blood flowing in a channel of height = 40 μm and hematocrit = 20%. To quantify platelet margination, we define the percentage of platelet margination (ϕ_p) by the ratio of number of platelets in the cell-free region to the total number of platelets in the simulated blood. A value of $\phi_p = 84\%$ is obtained for the NRBC and PLT suspensions flowing at $\dot{\gamma}_w = 1000\ s^{-1}$.

For diabetic blood flow simulation of DRBC suspensions, a relatively lower platelet concentration in the CFL and $\phi_p = 74\%$ are observed (Fig. 2 *b*). The RBC deformability is crucial to the platelet transport, and the impaired deformability of DRBCs compared to NRBCs may cause weaker platelet margination toward the wall. There is in vitro evidence showing that the presence of rigid RBCs interferes with the WBC recruitment and platelet margination (82,83). In addition, Kumar and Graham have presented a detailed analysis of the segregation mechanism incorporating binary mixtures of capsules with different rigidities by performing a computational study with the boundary integral method (84). They found that the degree of segregation increases with increasing rigidity difference between two types of capsules, which is also due to the increase in the heterogenous pair collisions between the stiff and floppy (deformable) capsules. In our study, platelet margination in T2DM RBC suspensions is found to increase when the platelet size is enlarged. As shown in the platelet concentration profiles in Fig. 2, *b* and *c*, the concentration of PLT* in the CFL region is higher than that of PLT for both cases with identical hematocrit and flowrate. We also conducted a sensitivity study for the platelet transport with different MPV values (MPV = 6–12 fL) in the diabetic blood flow, confirming that the percentage of platelet margination increases monotonically with increasing MPV (Fig. 2 *d*). The size-dependent margination of particles in blood flow has been found in a number of experimental and computational studies (53,85–89). For example, it is found that spherical microparticles (diameter > 0.5 μm) are marginated significantly more than nanoparticles (diameter < 0.5 μm), and those small-sized particles are easily trapped in the RBC core. Particle sizes close to the CFL thickness may have the optimized sizes for efficient margination and also for drug-delivery systems (90). Comparing the RBC distributions in the vessel, there is no distinct difference between the NRBC and DRBC suspensions as shown in Fig. 2, *a–c*. This result is also in agreement with the studies by Kumar and Graham, who showed that an alteration in the membrane rigidity of floppy capsules has minor impact on their distribution (84).

We have also performed simulations of blood flow with a binary mixture of 50% PLTs and 50% PLT*s suspended in DRBCs (Fig. 3). The normalized cell-center distribution of DRBCs is similar to the previous results, and the platelet concentration profile of the mixture (Fig. 3 *a*) exhibits a similar platelet distribution to that of Fig. 2 *c*, however, with relatively weaker platelet margination for which the values are somewhat in between those of Fig. 2, *b* and *c*. To compare the migration velocity of platelets, we plot the trajectories of all modeled PLTs and PLT*s with respect to time and highlight two representative trajectories. The blue trajectory represents the PLT, whereas the red one corresponds to the PLT*. Note that all platelets are initially placed away from the vessel wall with a minimal distance of 5 μm. As shown in Fig. 3 *b*, the larger PLT*s migrate to the wall faster than PLTs, and most marginated platelets show an abrupt lateral displacement once they reach closer to the edge of RBC core. This rapid margination, named "waterfall phenomenon," was observed in other numerical simulations as well (44,88). In addition, we estimate the transient percentage of platelet margination of two platelet sizes see (Fig. 3 *c*). Clearly, there is a higher tendency of margination for PLT*s than PLTs at the beginning ~0.1 s, but the difference in the degree of margination becomes smaller at later times.

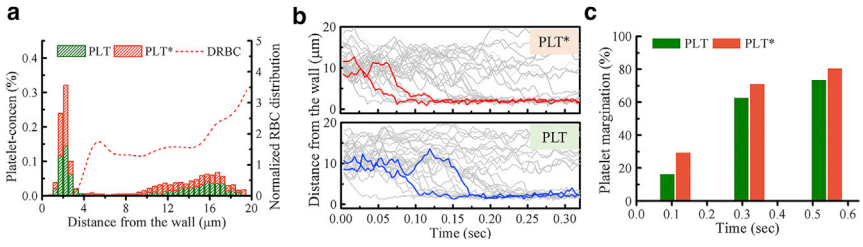

FIGURE 3 DRBCs with a mixture of 50% PLTs and 50% PLT*s flowing in a vessel at $\dot{\gamma}_w = 1000\ s^{-1}$ and $H_{ct} = 20\%$. (*a*) Concentration profiles of RBCs and platelets, in which the histogram plot is adopted for the platelet concentration profile. (*b*) The trajectories of PLTs and PLT*s with time. Two representative trajectories (the 4th and 10th marginated platelets) are shown in blue lines for PLT and in red lines for PLT*. (*c*) Temporal evolution of the percentage of PLT and PLT* marginations based on their count. To see this figure in color, go online.

Effects of flowrate and blood hematocrit

First, we investigate the effect of flowrate on RBC and platelet distributions in a vessel in which blood hematocrit $H_{ct} = 20\%$ is fixed for three different cell type suspensions: NRBCs+PLTs, DRBCs+PLTs and DRBCs+PLT*s. The RBC distribution and CFL thickness in Fig. 4, *a–c* seems to be independent of the variation of $\dot{\gamma}_w$ from 1000 s^{-1} (previous case) to 600 s^{-1}. This is in agreement with the result of Freund et al. (80,91) that showed the CFL thickness is independent of flowrate when the wall shear rate is high (>100 s^{-1}). Interestingly, although the normalized RBC distributions do not show significant difference at $\dot{\gamma}_w = 1000$ and 600 s^{-1}, a decrease in the platelet concentration within the CFL region has been found in all blood cell suspensions. For a better comparison of the degree of platelet margination in all flow conditions, we estimate ϕ_p (see the values shown in Fig. 4 *d*). There is ~6–10% decrease in ϕ_p when wall shear rate is reduced from $\dot{\gamma}_w = 1000$ to 600 s^{-1}. The decrease in platelet margination with decreasing wall shear rate ($\dot{\gamma}_w$) is thought to be the result of reduction in the collision frequencies between RBCs and platelets. In addition, for the case of normal blood flow (NRBCs + PLTs), ϕ_p is close to the diabetic blood flow (DRBCs + PLT*s), and both are higher than the ϕ_p value for cell suspensions containing DRBCs and PLTs. In comparison with the normal platelets, our results indicate that the larger platelets (commonly observed in T2DM) have a stronger tendency to migrate toward the vessel wall. This observation, together with the platelets' hyperreactivity in T2DM, could have significant contributions to increased thrombosis events in diabetic subjects.

Fig. 5 shows RBC and platelet concentration profiles of normal and diabetic blood flow at different mean blood hematocrit (H_{ct}), where $\dot{\gamma}_w = 1000$ s^{-1}. When there is no presence of RBCs ($H_{ct} = 0\%$), platelets (either PLTs or PLT*s) are concentrated around the center of the vessel (see *gray histograms* in Fig. 5, *a* and *b*). This effect has also been observed in the experiments of particle transport in microchannels without RBCs (53,92). When RBCs are introduced, the CFL is formed because of the wall-induced migration driving soft RBCs away from the wall, whereas platelets drift toward the wall because of the shear-induced diffusion caused by their heterogeneous collisions with the RBCs. The NRBC and DRBC concentration profiles in Fig. 5, *a* and *b* indicate that the RBC core is expanded and CFL thickness is decreased with increasing blood hematocrit H_{ct}. In addition, as H_{ct} increases, the near-wall peaks of platelet concentration shift toward the wall and the percentage of platelet margination (ϕ_p) increases and reaches ~85% when $H_{ct} \geq 20\%$ (see the platelet concentration profiles and ϕ_p estimated for different H_{ct} in Fig. 5, *a–c*). We also present the snapshots of diabetic blood flow with mean hematocrit from $H_{ct} = 0$ to 25% for a clear visualization of DRBCS and PLT*s distributions in the vessel at time = 0.54 s (Fig. 5 *d*).

Effects of platelet shape and WBC count

In general, an inactivated (resting) platelet has an oblate spheroid shape of AR = 0.25–0.5 (63). We further perform simulations to study the effects of platelet shape on its margination by varying the AR = 0.28, 0.38, and 0.5.

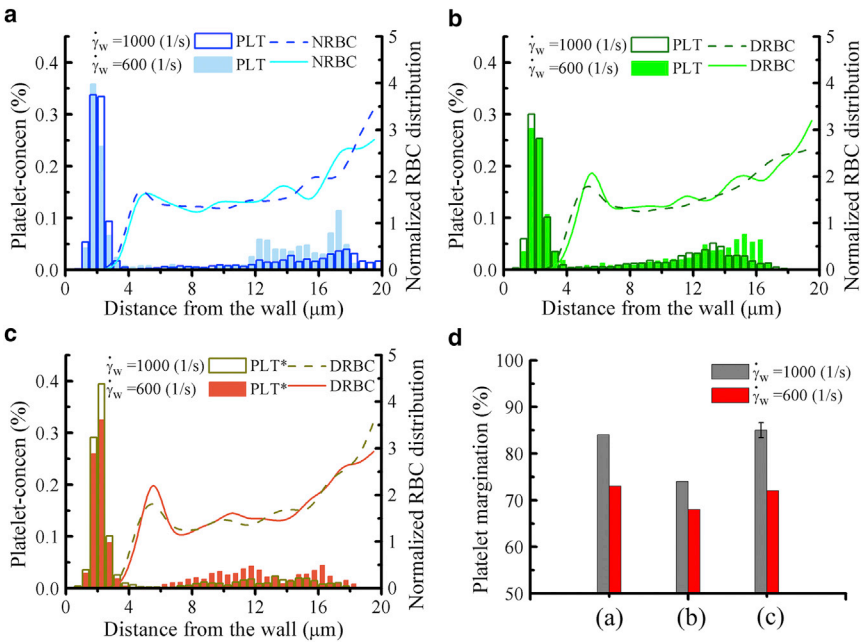

FIGURE 4 Effect of flowrate. Concentration profiles of platelets and RBCs in the vessel ($D_t = 40$ μm) are shown, in which cell suspensions of (*a*) NRBCs + PLTs, (*b*) DRBCs + PLTs, and (*c*) DRBCs + PLT*s with identical $H_{ct} = 20\%$ but at different wall shear rates $\dot{\gamma}_w = 600$ and 1000 s^{-1} are considered. (*d*) The percentage of marginated platelet ϕ_p is shown for all three cases. To see this figure in color, go online.

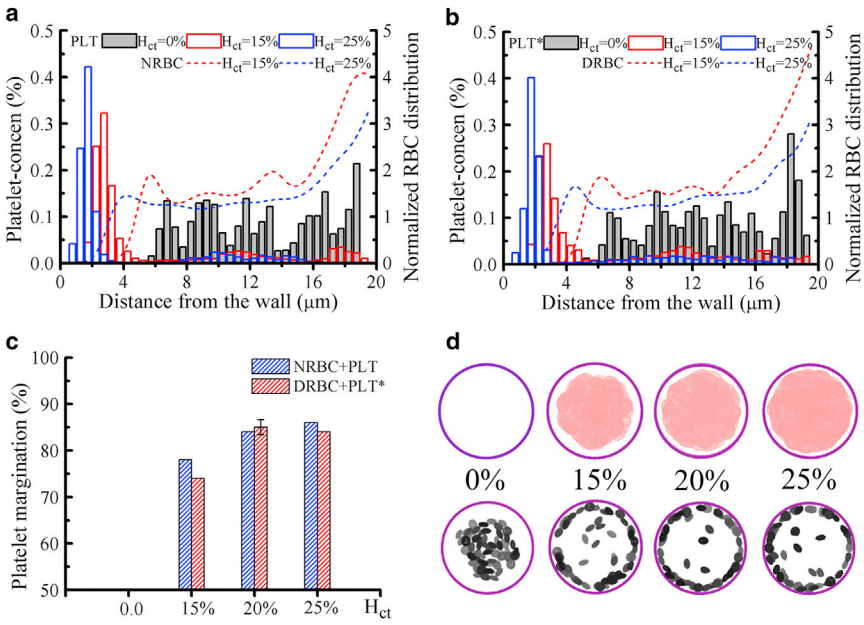

FIGURE 5 Effect of blood hematocrit at $\dot{\gamma}_w = 1000\ s^{-1}$. Concentration profiles of platelets and RBCs in the vessel ($D_t = 40\ \mu m$) for (*a*) $H_{ct} = 0\%$ and NRBC + PLT for $H_{ct} = 15$ and 25% and (*b*) $H_{ct} = 0\%$ and DRBC + PLT* for $H_{ct} = 15$ and 25%. (*c*) The percentage of marginated platelets ϕ_p for normal and diabetic cell suspensions at different H_{ct}. (*d*) Front views of the vessel to show the distributions of DRBCs (*upper row*) and PLT*s (*lower row*) are shown with $H_{ct} = 0$, 15, 20, and 25% at time = 0.54 s. To see this figure in color, go online.

Fig. 6 presents platelet concentration profiles and the percentage of platelet margination of PLT* (MPV = 12 fL) for different AR values suspended in the DRBCs. It is clear that the highest near-wall concentration for PLT* is achieved for AR = 0.38. The significantly flatter oblate shapes with AR = 0.28 and the tumid oblate shapes with AR = 0.5 for platelets show lower near-wall accumulations. This result has also been reported recently by Vahidkhah and Bagchi (93) for healthy blood, in which a higher margination rate was observed for moderately aspherical particles but not for the highly aspherical ones. In addition, we observe that platelets with AR = 0.28 have less margination propensity with decreasing blood hematocrit (see Fig. 6 *b*). Different from the hematocrit effect analysis on the margination of moderate-oblate-shaped PLT*s (see above), flat-oblate-shaped PLT*s are less sensitive to the change of blood hematocrit. Nevertheless, many studies have found higher margination and binding probabilities for particles with aspherical shape than those with spherical shape (94–96). Platelets with their naturally oblate spheroid shape are endowed with a larger contact area compared to the spherical particles of the same volume.

WBCs, as an important part of immune system, are subject to a recruitment process from the blood stream to a site of inflammation, followed by a number of interactions with endothelium via receptor-ligand bindings (77–79). For weak or few interactions, WBCs roll along the endothelium, whereas for strong interactions such as the integrin-mediated bonds, WBCs can be firmly attached on the endothelial surface (97). Similar to platelets, WBCs are substantially stiffer than RBCs, and their margination occurs because of the heterogeneous collisions with RBCs. WBCs margination is prominent in postcapillary venules with a characteristic of low blood flowrate in contrast to the massive number of marginated platelets extensively observed in arterioles (28). However, induced leukocyte-arterial endothelium interactions and the WBC recruitments

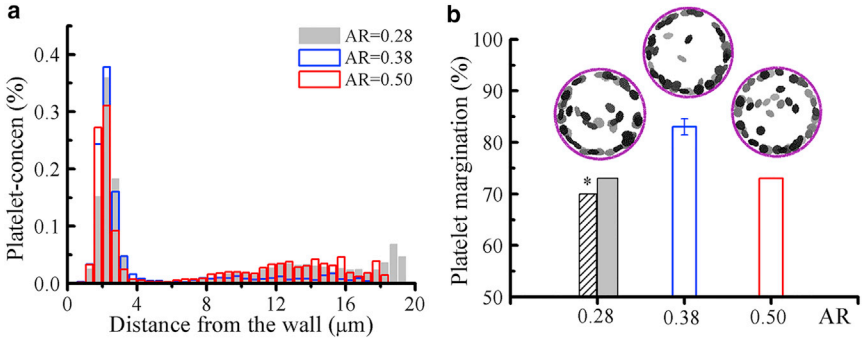

FIGURE 6 Effect of platelet shape with $\dot{\gamma}_w = 1000\ s^{-1}$ and $H_{ct} = 20\%$. (*a*) Concentration profiles of platelets in a vessel with DRBCs and PLT* at different AR values. (*b*) The percentage of marginated platelets ϕ_p for each AR value. The histogram with * is the result for platelets with AR = 0.28 and blood hematocrit $H_{ct} = 15\%$. Snapshots show the front views of vessel with different PLT*s suspended in DRBCs, for which $H_{ct} = 20\%$. To see this figure in color, go online.

into atherosclerotic lesions in arteries have been revealed by ex vivo experiments (98,99).

Considering that the blood flow disturbance in small vessels may be caused by the presence of WBCs, we therefore include them into the simulations having three dynamic states often observed in blood vessels: circulating freely in the blood stream, rolling on the wall, and firm adhesion to the wall. The platelet concentration profiles and the percentage of platelet margination in Fig. 7, *a* and *b* show no clear difference in the near-wall concentration of PLT*s between the blood flows with freely flowing WBCs and without the presence of WBCs. However, we observe that platelet margination is impaired when WBCs emerge near the vessel wall, where more reduction in platelets margination is observed with more rolling or adherent WBCs close to the wall. The solid bars in Fig. 7 *b* correspond to a single WBC, whereas empty bars correspond to three WBCs in the domain. We also present three snapshots of near-wall platelet dynamics when platelets transport close to an adhered WBC (see Fig. 7 *c* and Videos S1, S2, and S3). The platelets that come in contact with an adhered WBC either slide from the top or on the side of the WBC, after which they undergo flipping motions (Videos S1 and S2). The platelets that move close to an adhered WBC only exhibit flipping motions in the direction of flow because of their discoid shapes (Video S3). In a flow system with adhered WBCs, platelet transport toward vessel walls is hindered because of the flow resistance induced by the adhered WBCs. However, the cell-cell contacts between platelets and WBCs might be enhanced because of the sliding motion of platelets on the surface of an adhered WBC. The sliding motion of platelets can facilitate the adhesive interactions between platelet CD62 and leukocyte P-selectin glycoprotein ligand-1, which further leads to platelet-WBC aggregations (100,101). Here, we consider only hydrodynamic cell-cell interactions, and the effects of adhesive dynamics will be studied in our future work.

CONCLUSIONS

T2DM is strongly associated with the accelerated development of atherothrombosis and cardiovascular diseases (1). In this study, we perform high-fidelity blood flow simulations to investigate RBC and platelet transport in the cylindrical vessels resembling small arterioles under healthy and diabetic conditions. In particular, diabetic blood is composed of T2DM RBCs and T2DM platelets. We do not model cell-cell or cell-wall adhesive interactions to study systematically the hydrodynamic interactions that induce margination. We employ the DPD method to seamlessly model RBCs, platelets, WBCs, plasma, and the vessel wall. We first validate the DPD model using experimental data for margination of microbeads (three different sizes) in channel blood flow by Carboni et al. (53). We found that, in agreement with the experiments, margination of micro-beads increases with size and shear rate. We have introduced and validated a T2DM RBC model in our previous work (48). Here, we adopted the same red cell model for modeling the diabetic blood, whereas a T2DM platelet model is built based on the parameters informed by the clinical blood analysis of 64 diabetic patients. According to the statistical analysis for the blood characteristics, the average MPV in diabetics (10.0 $\pm$ 1.26 fL) is higher than the average MPV (9.2 $\pm$ 1.70 fL) in nondiabetics. To distinguish the platelet margination in diabetic blood from that in normal blood, we chose the extreme values of MPV $=$ 6 fL for normal platelets and MPV $=$ 12 fL for T2DM platelets. Similarly, for RBCs, we considered their volume (MCV) to have values close to mean value for normal blood and extreme value for diabetic blood. Our blood flow simulations show that platelet margination in whole blood is a very complex and multifactorial process, affected by the biomechanical properties of cells and their shape and size as well as blood flowrate and hematocrit. For diabetic blood flows,

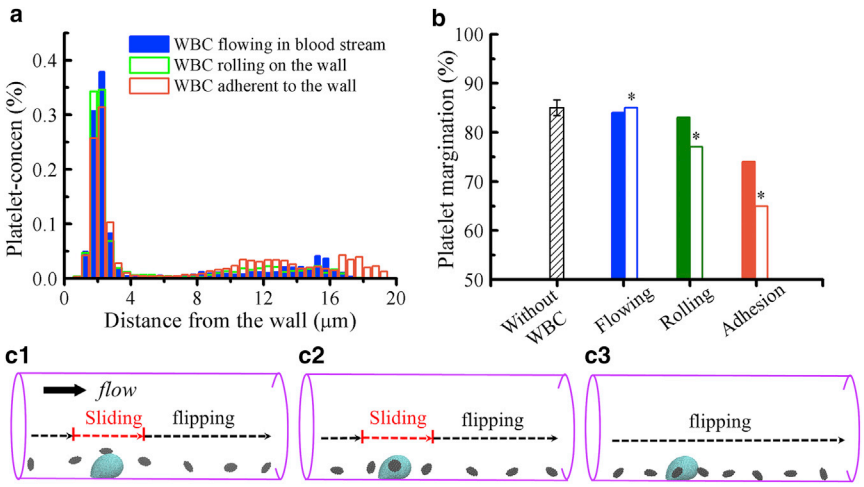

FIGURE 7 Effect of WBC dynamics at $\dot{\gamma}_w = 1000\ s^{-1}$ and $H_{ct} = 20\%$. (*a*) Concentration profiles of platelets in the vessel with a WBC flowing in the blood stream, rolling on the wall, and adhered to the wall are shown. (*b*) The percentage of marginated platelets ϕ_p in the blood flow without WBCs and with a WBC under different dynamical states, for which the * label on the histograms denotes the blood contains three WBCs. (*c*) Snapshots of near-wall platelet dynamics in a blood flow condition with an adhered WBC showing a representative platelet sliding on the top of the WBC (*c1*), sliding on the side of the WBC (*c2*), and flipping nearby the WBC (*c3*). DRBCs and PLT*s are used in these simulations. To see this figure in color, go online.

we found two competing effects on platelet margination: T2DM RBCs with less deformability compared to normal RBCs contribute to reduced heterogenous collisions, hence impairing platelet margination. On the other hand, T2DM platelets with higher MPV lead to increased margination. We also conducted sensitivity studies for the platelet transport with different MPV values in the diabetic blood flow and found that the percentage of platelet margination increases monotonically with increasing MPV. Similar to healthy blood flow, platelet margination in diabetic blood flow is increased with increasing flowrate and blood hematocrit. Considering the effect of platelet shape on its margination, we found that the highest near-wall accumulation of T2DM platelets are those with moderate AR. We further took into account the WBC dynamics in blood and found that WBC rolling and WBC adhesion tend to decrease platelet margination based on hydrodynamic interactions. In future work, we will include the effects of cell-cell adhesive interactions as well as cell-wall interactions, which could change some of the quantitative findings of this work. Elucidating the predictors of platelet margination and the highest near-wall accumulation of platelets in diabetics will not only allow for the creation of algorithms predicting CVD risk among diabetics but could also point to specific molecular pathways that could lend themselves to predictive or therapeutic interventions.

SUPPORTING MATERIAL

Supporting Materials and Methods, three figures, four tables, and three videos are available at http://www.biophysj.org/biophysj/supplemental/S0006-3495(18)31008-7.

AUTHOR CONTRIBUTIONS

H.-Y.C., A.Y., X.L., C.S.M., and G.E.K. conceived and designed the research. H.-Y.C. and A.Y. carried out all simulations. K.A.A.D. provided clinical data. H.-Y.C., A.Y., X.L., C.S.M., and G.E.K. analyzed the data. H.-Y.C., A.Y., X.L., C.S.M., and G.E.K. wrote the article.

ACKNOWLEDGMENTS

H.-Y.C. would like to thank Dr. Yu-Hang Tang for the use of an in-house-developed code Ermine and Dr. Zhen Li for the code for a cell generator used in this study.

The work described in this article was supported by National Institutes of Health grants U01HL114476 and U01HL116323. C.S.M. also acknowledges support from National Institute of Diabetes and Digestive and Kidney Diseases grant K24DK081913. Computations were performed using resources and services at the Center for Computation and Visualization at Brown University, the Oak Ridge Leadership Computing Facility/Argonne Leadership Computing Facility computational resources at Oak Ridge National Laboratory/Argonne National Laboratory through an ASCR Leadership Computing Challenge award, and the National Science Foundation Extreme Science and Engineering Discovery Environment resources through award No. TG-DMS140007.

REFERENCES

1. King, R. J., and P. J. Grant. 2016. Diabetes and cardiovascular disease: pathophysiology of a life-threatening epidemic. *Herz.* 41:184–192.
2. Mantzoros, C. S. 2009. Methods for classifying, diagnosing, and monitoring type II diabetes. Nutrition and Metabolism. Springer, pp. 385–391.
3. Grant, P. J. 2007. Diabetes mellitus as a prothrombotic condition. *J. Intern. Med.* 262:157–172.
4. Alzahrani, S. H., and R. A. Ajjan. 2010. Coagulation and fibrinolysis in diabetes. *Diab. Vasc. Dis. Res.* 7:260–273.
5. Ferroni, P., S. Basili, …, G. Davì. 2004. Platelet activation in type 2 diabetes mellitus. *J. Thromb. Haemost.* 2:1282–1291.
6. Vinik, A. I., T. Erbas, …, G. L. Pittenger. 2001. Platelet dysfunction in type 2 diabetes. *Diabetes Care.* 24:1476–1485.
7. Ferreiro, J. L., J. A. Gómez-Hospital, and D. J. Angiolillo. 2010. Platelet abnormalities in diabetes mellitus. *Diab. Vasc. Dis. Res.* 7:251–259.
8. Kim, J. H., H. Y. Bae, and S. Y. Kim. 2013. Clinical marker of platelet hyperreactivity in diabetes mellitus. *Diabetes Metab. J.* 37:423–428.
9. Yeom, E., H. Byeon, and S. J. Lee. 2016. Effect of diabetic duration on hemorheological properties and platelet aggregation in streptozotocin-induced diabetic rats. *Sci. Rep.* 6:21913.
10. Sterner, G., J. Carlson, and G. Ekberg. 1998. Raised platelet levels in diabetes mellitus complicated with nephropathy. *J. Intern. Med.* 244:437–441.
11. Sharpe, P. C., and T. Trinick. 1993. Mean platelet volume in diabetes mellitus. *Q. J. Med.* 86:739–742.
12. Shilpi, K., and R. M. Potekar. 2018. A study of platelet indices in type 2 diabetes mellitus patients. *Indian J. Hematol. Blood Transfus.* 34:115–120.
13. Papanas, N., G. Symeonidis, …, G. Lakasas. 2004. Mean platelet volume in patients with type 2 diabetes mellitus. *Platelets.* 15:475–478.
14. Tavil, Y., N. Sen, …, A. Abaci. 2010. Coronary heart disease is associated with mean platelet volume in type 2 diabetic patients. *Platelets.* 21:368–372.
15. Gasparyan, A. Y., L. Ayvazyan, …, G. D. Kitas. 2011. Mean platelet volume: a link between thrombosis and inflammation? *Curr. Pharm. Des.* 17:47–58.
16. Vizioli, L., S. Muscari, and A. Muscari. 2009. The relationship of mean platelet volume with the risk and prognosis of cardiovascular diseases. *Int. J. Clin. Pract.* 63:1509–1515.
17. Hathcock, J. J. 2006. Flow effects on coagulation and thrombosis. *Arterioscler. Thromb. Vasc. Biol.* 26:1729–1737.
18. Diamond, S. L. 2016. Systems analysis of thrombus formation. *Circ. Res.* 118:1348–1362.
19. Monroe, D. M., M. Hoffman, and H. R. Roberts. 2002. Platelets and thrombin generation. *Arterioscler. Thromb. Vasc. Biol.* 22:1381–1389.
20. Burke, A. P., F. D. Kolodgie, …, R. Virmani. 2004. Morphologic findings of coronary atherosclerotic plaques in diabetics: a postmortem study. *Arterioscler. Thromb. Vasc. Biol.* 24:1266–1271.
21. Bagchi, P. 2007. Mesoscale simulation of blood flow in small vessels. *Biophys. J.* 92:1858–1877.
22. Lei, H., D. A. Fedosov, …, G. E. Karniadakis. 2013. Blood flow in small tubes: quantifying the transition to the non-continuum regime. *J. Fluid Mech.* 722:214–239.
23. Fedosov, D. A., B. Caswell, …, G. E. Karniadakis. 2010. Blood flow and cell-free layer in microvessels. *Microcirculation.* 17:615–628.
24. Fahraeus, R., and T. Lindqvist. 1931. The viscosity of the blood in narrow capillary tubes. *Am. J. Physiol.* 96:562–568.
25. Tangelder, G. J., D. W. Slaaf, and R. S. Reneman. 1982. Fluorescent labeling of blood platelets in vivo. *Thromb. Res.* 28:803–820.

26. Tangelder, G. J., H. C. Teirlinck, …, R. S. Reneman. 1985. Distribution of blood platelets flowing in arterioles. *Am. J. Physiol.* 248: H318–H323.

27. Woldhuis, B., G. J. Tangelder, …, R. S. Reneman. 1992. Concentration profile of blood platelets differs in arterioles and venules. *Am. J. Physiol.* 262:H1217–H1223.

28. Kumar, A., and M. D. Graham. 2012. Margination and segregation in confined flows of blood and other multicomponent suspensions. *Soft Matter.* 8:10536–10548.

29. Zhao, R., M. V. Kameneva, and J. F. Antaki. 2007. Investigation of platelet margination phenomena at elevated shear stress. *Biorheology.* 44:161–177.

30. Aarts, P. A., S. A. van den Broek, …, R. M. Heethaar. 1988. Blood platelets are concentrated near the wall and red blood cells, in the center in flowing blood. *Arteriosclerosis.* 8:819–824.

31. Fitzgibbon, S., A. P. Spann, …, E. S. G. Shaqfeh. 2015. In vitro measurement of particle margination in the microchannel flow: effect of varying hematocrit. *Biophys. J.* 108:2601–2608.

32. Tilles, A. W., and E. C. Eckstein. 1987. The near-wall excess of platelet-sized particles in blood flow: its dependence on hematocrit and wall shear rate. *Microvasc. Res.* 33:211–223.

33. Yeh, C., and E. C. Eckstein. 1994. Transient lateral transport of platelet-sized particles in flowing blood suspensions. *Biophys. J.* 66:1706–1716.

34. Sweet, C. R., S. Chatterjee, …, M. Alber. 2011. Modelling platelet-blood flow interaction using the subcellular element Langevin method. *J. R. Soc. Interface.* 8:1760–1771.

35. Xu, Z., O. Kim, …, M. Alber. 2012. Multiscale models of thrombogenesis. *Wiley Interdiscip. Rev. Syst. Biol. Med.* 4:237–246.

36. Einav, S., and D. Bluestein. 2004. Dynamics of blood flow and platelet transport in pathological vessels. *Ann. N. Y. Acad. Sci.* 1015:351–366.

37. Rack, K., V. Huck, …, G. Gompper. 2017. Margination and stretching of von Willebrand factor in the blood stream enable adhesion. *Sci. Rep.* 7:14278.

38. Zhao, H., and E. S. Shaqfeh. 2011. Shear-induced platelet margination in a microchannel. *Phys. Rev. E Stat. Nonlin. Soft Matter Phys.* 83:061924.

39. Crowl, L. M., and A. L. Fogelson. 2010. Computational model of whole blood exhibiting lateral platelet motion induced by red blood cells. *Int. J. Numer. Methods Biomed. Eng.* 26:471–487.

40. Crowl, L., and A. L. Fogelson. 2011. Analysis of mechanisms for platelet near-wall excess under arterial blood flow conditions. *J. Fluid Mech.* 676:348–375.

41. Reasor, D. A., Jr., M. Mehrabadi, …, C. K. Aidun. 2013. Determination of critical parameters in platelet margination. *Ann. Biomed. Eng.* 41:238–249.

42. Mehrabadi, M., D. N. Ku, and C. K. Aidun. 2016. Effects of shear rate, confinement, and particle parameters on margination in blood flow. *Phys. Rev. E.* 93:023109.

43. Mehrabadi, M., D. N. Ku, and C. K. Aidun. 2015. A continuum model for platelet transport in flowing blood based on direct numerical simulations of cellular blood flow. *Ann. Biomed. Eng.* 43:1410–1421.

44. Vahidkhah, K., S. L. Diamond, and P. Bagchi. 2014. Platelet dynamics in three-dimensional simulation of whole blood. *Biophys. J.* 106: 2529–2540.

45. Soares, J. S., C. Gao, …, D. Bluestein. 2013. Simulation of platelets suspension flowing through a stenosis model using a dissipative particle dynamics approach. *Ann. Biomed. Eng.* 41:2318–2333.

46. Yazdani, A., and G. E. Karniadakis. 2016. Sub-cellular modeling of platelet transport in blood flow through microchannels with constriction. *Soft Matter.* 12:4339–4351.

47. Chesnutt, J. K., and H. C. Han. 2013. Platelet size and density affect shear-induced thrombus formation in tortuous arterioles. *Phys. Biol.* 10:056003.

48. Chang, H. Y., X. Li, and G. E. Karniadakis. 2017. Modeling of biomechanics and biorheology of red blood cells in type 2 diabetes mellitus. *Biophys. J.* 113:481–490.

49. Pettersson, U. S., G. Christoffersson, …, M. Phillipson. 2011. Increased recruitment but impaired function of leukocytes during inflammation in mouse models of type 1 and type 2 diabetes. *PLoS One.* 6:e22480.

50. Algenstaedt, P., C. Schaefer, …, N. Hansen-Algenstaedt. 2003. Microvascular alterations in diabetic mice correlate with level of hyperglycemia. *Diabetes.* 52:542–549.

51. Galkina, E., and K. Ley. 2006. Leukocyte recruitment and vascular injury in diabetic nephropathy. *J. Am. Soc. Nephrol.* 17:368–377.

52. Hess, K., and P. J. Grant. 2011. Inflammation and thrombosis in diabetes. *Thromb. Haemost.* 105 (*Suppl 1*):S43–S54.

53. Carboni, E. J., B. H. Bognet, …, A. W. K. Ma. 2016. Direct tracking of particles and quantification of margination in blood flow. *Biophys. J.* 111:1487–1495.

54. Pivkin, I. V., and G. E. Karniadakis. 2008. Accurate coarse-grained modeling of red blood cells. *Phys. Rev. Lett.* 101:118105.

55. Fedosov, D. A., B. Caswell, and G. E. Karniadakis. 2010. Systematic coarse-graining of spectrin-level red blood cell models. *Comput. Methods Appl. Mech. Eng.* 199:1937–1948.

56. Bokori-Brown, M., P. G. Petrov, …, C. P. Winlove. 2016. Red blood cell susceptibility to pneumolysin: correlation with membrane biochemical and physical properties. *J. Biol. Chem.* 291:10210–10227.

57. Jin, H., X. Xing, …, J. Cai. 2010. Detection of erythrocytes influenced by aging and type 2 diabetes using atomic force microscope. *Biochem. Biophys. Res. Commun.* 391:1698–1702.

58. Evan-Wong, L. A., and R. J. Davidson. 1983. Raised Coulter mean corpuscular volume in diabetic ketoacidosis, and its underlying association with marked plasma hyperosmolarity. *J. Clin. Pathol.* 36:334–336.

59. Morse, E. E., G. Kalache, …, R. Stockwell. 1981. Increased electronic mean corpuscular volume induced by marked hyperglycemia. *Ann. Clin. Lab. Sci.* 11:184–187.

60. Agrawal, R., T. Smart, …, C. Pavesio. 2016. Assessment of red blood cell deformability in type 2 diabetes mellitus and diabetic retinopathy by dual optical tweezers stretching technique. *Sci. Rep.* 6:15873.

61. Lee, S., H. Park, …, Y. Park. 2017. Refractive index tomograms and dynamic membrane fluctuations of red blood cells from patients with diabetes mellitus. *Sci. Rep.* 7:1039.

62. Kolesnikova, I. V., S. V. Potapov, …, K. A. Semyanov. 2006. Determination of volume, shape and refractive index of individual blood platelets. *J. Quant. Spectrosc. Radiat. Transf.* 102:37–45.

63. Michelson, A. 2011. Platelets. Elsevier Science, New York.

64. Fagard, R. H. 2009. Smoking amplifies cardiovascular risk in patients with hypertension and diabetes. *Diabetes Care.* 32 (*Suppl 2*):S429–S431.

65. Haga, J. H., A. J. Beaudoin, …, J. Strony. 1998. Quantification of the passive mechanical properties of the resting platelet. *Ann. Biomed. Eng.* 26:268–277.

66. Wu, Z., Z. Xu, …, M. Alber. 2014. Three-dimensional multi-scale model of deformable platelets adhesion to vessel wall in blood flow. *Philos Trans A Math Phys Eng Sci.* 372:20130380.

67. Radmacher, M., M. Fritz, …, P. K. Hansma. 1996. Measuring the viscoelastic properties of human platelets with the atomic force microscope. *Biophys. J.* 70:556–567.

68. Du Plooy, J. N., A. Buys, …, E. Pretorius. 2013. Comparison of platelet ultrastructure and elastic properties in thrombo-embolic ischemic stroke and smoking using atomic force and scanning electron microscopy. *PLoS One.* 8:e69774.

69. Skorczewski, T., L. C. Erickson, and A. L. Fogelson. 2013. Platelet motion near a vessel wall or thrombus surface in two-dimensional whole blood simulations. *Biophys. J.* 104:1764–1772.

70. AlMomani, T., H. S. Udaykumar, …, K. B. Chandran. 2008. Micro-scale dynamic simulation of erythrocyte-platelet interaction in blood flow. *Ann. Biomed. Eng.* 36:905–920.

71. Lei, H., and G. E. Karniadakis. 2013. Probing vasoocclusion phenomena in sickle cell anemia via mesoscopic simulations. *Proc. Natl. Acad. Sci. USA.* 110:11326–11330.

72. Jadhav, S., C. D. Eggleton, and K. Konstantopoulos. 2005. A 3-D computational model predicts that cell deformation affects selectin-mediated leukocyte rolling. *Biophys. J.* 88:96–104.

73. Linderkamp, O., P. Ruef, …, G. F. Hoffmann. 1999. Impaired deformability of erythrocytes and neutrophils in children with newly diagnosed insulin-dependent diabetes mellitus. *Diabetologia.* 42: 865–869.

74. Yedgar, S., A. Koshkaryev, and G. Barshtein. 2002. The red blood cell in vascular occlusion. *Pathophysiol. Haemost. Thromb.* 32:263–268.

75. Fedosov, D. A., W. Pan, …, G. E. Karniadakis. 2011. Predicting human blood viscosity in silico. *Proc. Natl. Acad. Sci. USA.* 108: 11772–11777.

76. Bessman, J. D., L. J. Williams, and P. R. J. Gilmer, Jr. 1981. Mean platelet volume. The inverse relation of platelet size and count in normal subjects, and an artifact of other particles. *Am. J. Clin. Pathol.* 76:289–293.

77. McLeod, D. S., D. J. Lefer, …, G. A. Lutty. 1995. Enhanced expression of intracellular adhesion molecule-1 and P-selectin in the diabetic human retina and choroid. *Am. J. Pathol.* 147:642–653.

78. Lawrence, M. B., and T. A. Springer. 1991. Leukocytes roll on a selectin at physiologic flow rates: distinction from and prerequisite for adhesion through integrins. *Cell.* 65:859–873.

79. Blankenberg, S., S. Barbaux, and L. Tiret. 2003. Adhesion molecules and atherosclerosis. *Atherosclerosis.* 170:191–203.

80. Zhao, H., E. S. Shaqfeh, and V. Narsimhan. 2012. Shear-induced particle migration and margination in a cellular suspension. *Phys. Fluids.* 24:011902.

81. Lipowsky, H. H., S. Usami, and S. Chien. 1980. In vivo measurements of "apparent viscosity" and microvessel hematocrit in the mesentery of the cat. *Microvasc. Res.* 19:297–319.

82. Gutierrez, M., M. B. Fish, …, O. Eniola-Adefeso. 2018. Presence of rigid red blood cells in blood flow interferes with the vascular wall adhesion of leukocytes. *Langmuir.* 34:2363–2372.

83. Watts, T., M. Barigou, and G. B. Nash. 2013. Comparative rheology of the adhesion of platelets and leukocytes from flowing blood: why are platelets so small? *Am. J. Physiol. Heart Circ. Physiol.* 304:H1483–H1494.

84. Kumar, A., and M. D. Graham. 2011. Segregation by membrane rigidity in flowing binary suspensions of elastic capsules. *Phys. Rev. E Stat. Nonlin. Soft Matter Phys.* 84:066316.

85. Namdee, K., A. J. Thompson, …, O. Eniola-Adefeso. 2013. Margination propensity of vascular-targeted spheres from blood flow in a microfluidic model of human microvessels. *Langmuir.* 29:2530–2535.

86. Charoenphol, P., R. B. Huang, and O. Eniola-Adefeso. 2010. Potential role of size and hemodynamics in the efficacy of vascular-targeted spherical drug carriers. *Biomaterials.* 31:1392–1402.

87. Lee, S. Y., M. Ferrari, and P. Decuzzi. 2009. Shaping nano-/micro-particles for enhanced vascular interaction in laminar flows. *Nanotechnology.* 20:495101.

88. Lee, T. R., M. Choi, …, P. Decuzzi. 2013. On the near-wall accumulation of injectable particles in the microcirculation: smaller is not better. *Sci. Rep.* 3:2079.

89. Müller, K., D. A. Fedosov, and G. Gompper. 2014. Margination of micro- and nano-particles in blood flow and its effect on drug delivery. *Sci. Rep.* 4:4871.

90. Müller, K., D. A. Fedosov, and G. Gompper. 2016. Understanding particle margination in blood flow - a step toward optimized drug delivery systems. *Med. Eng. Phys.* 38:2–10.

91. Freund, J. B., and M. Orescanin. 2011. Cellular flow in a small blood vessel. *J. Fluid Mech.* 671:466–490.

92. D'Apolito, R., G. Tomaiuolo, …, S. Guido. 2015. Red blood cells affect the margination of microparticles in synthetic microcapillaries and intravital microcirculation as a function of their size and shape. *J. Control. Release.* 217:263–272.

93. Vahidkhah, K., and P. Bagchi. 2015. Microparticle shape effects on margination, near-wall dynamics and adhesion in a three-dimensional simulation of red blood cell suspension. *Soft Matter.* 11:2097–2109.

94. Anselmo, A. C., C. L. Modery-Pawlowski, …, S. Mitragotri. 2014. Platelet-like nanoparticles: mimicking shape, flexibility, and surface biology of platelets to target vascular injuries. *ACS Nano.* 8:11243–11253.

95. van de Ven, A. L., P. Kim, …, P. Decuzzi. 2012. Rapid tumoritropic accumulation of systemically injected plateloid particles and their biodistribution. *J. Control. Release.* 158:148–155.

96. Muro, S., C. Garnacho, …, V. R. Muzykantov. 2008. Control of endothelial targeting and intracellular delivery of therapeutic enzymes by modulating the size and shape of ICAM-1-targeted carriers. *Mol. Ther.* 16:1450–1458.

97. Kubes, P., and S. M. Kerfoot. 2001. Leukocyte recruitment in the microcirculation: the rolling paradigm revisited. *News Physiol. Sci.* 16:76–80.

98. Ramos, C. L., Y. Huo, …, K. Ley. 1999. Direct demonstration of P-selectin- and VCAM-1-dependent mononuclear cell rolling in early atherosclerotic lesions of apolipoprotein E-deficient mice. *Circ. Res.* 84:1237–1244.

99. Kunkel, E. J., U. Jung, and K. Ley. 1997. TNF-alpha induces selectin-mediated leukocyte rolling in mouse cremaster muscle arterioles. *Am. J. Physiol.* 272:H1391–H1400.

100. Vandendries, E. R., B. C. Furie, and B. Furie. 2004. Role of P-selectin and PSGL-1 in coagulation and thrombosis. *Thromb. Haemost.* 92:459–466.

101. Elalamy, I., T. Chakroun, …, M. Hatmi. 2008. Circulating platelet-leukocyte aggregates: a marker of microvascular injury in diabetic patients. *Thromb. Res.* 121:843–848.

Biophysical Journal, Volume *115*

Supplemental Information

Quantifying Platelet Margination in Diabetic Blood Flow

Hung-Yu Chang, Alireza Yazdani, Xuejin Li, Konstantinos A.A. Douglas, Christos S. Mantzoros, and George Em Karniadakis

Supplementary Materials:

Quantifying Platelet Margination in Diabetic Blood Flow

H.-Y. Chang[1], A. Yazdani[1], X. J. Li[1], K. A. A. Douglas[2,3], C. S. Mantzoros[3], and G. E. Karniadakis[1,*]

[1] Division of Applied Mathematics, Brown University, Providence, RI 02912, U.S.A.
[2] S. Lepida Biomedical Laboratory, Athens 11146, Greece
[3] Division of Endocrinology, Diabetes and Metabolism, Beth Israel Deaconess Medical Center, Harvard Medical School, Boston, MA 02215, USA.
E-mail: George_Karniadakis@brown.edu.

Appendix A. Hydrodynamics and cell models

We employ dissipative particle dynamics (DPD) to model whole blood flow, *i.e.* plasma, red blood cells (RBCs), platelets and white blood cells (WBCs) in the microfluidic channels. The DPD method is a mesoscopic particle-based simulation technique, where each DPD particle represents a lump of molecules and interacts with other particles through soft pairwise forces. Since these interactions depend only on the relative positions and velocities, the resulting DPD fluids are Galilean invariant. Therefore, DPD can provide the correct hydrodynamic behavior of fluids at the mesoscale, and it has been successfully applied to study complex fluids (1, 2). The equation of motion for each particle i is governed by the sum of pair interactions $\mathbf{f}_i$ with the surrounding particles j and integrated using a velocity-Verlet algorithm. The time evolution of velocity ($\mathbf{v}_i$) and position ($\mathbf{r}_i$) of a particle i with mass m_i is determined by Newton's second law of motion:

$$\mathrm{d}\mathbf{r}_i = \mathbf{v}_i \,\mathrm{d}t\,; \quad \mathrm{d}\mathbf{v}_i = \mathbf{f}_i/m_i \,\mathrm{d}t. \tag{1}$$

In the classical DPD method, the total force $\mathbf{f}_i$ exerted on particle i by particle j is composed of a conservative force ($\mathbf{F}_{ij}^C$), a dissipative force ($\mathbf{F}_{ij}^D$), and a random force ($\mathbf{F}_{ij}^R$) given by

$$\mathbf{F}_{ij}^C = a_{ij}(1-\frac{r_{ij}}{r_c})\hat{\mathbf{r}}_{ij} \quad for \quad r_{ij} \le r_c; \quad 0 \quad for \quad r_{ij} > r_c, \tag{2}$$

$$\mathbf{F}_{ij}^D = \gamma\omega_d(r_{ij})(\hat{\mathbf{r}}_{ij}\cdot\hat{\mathbf{v}}_{ij})\hat{\mathbf{r}}_{ij}, \tag{3}$$

$$\mathbf{F}_{ij}^R = \sigma\omega_r(r_{ij})\frac{\zeta_{ij}}{\sqrt{dt}}\hat{\mathbf{r}}_{ij}, \tag{4}$$

where r_c is a cut-off radius, and a_{ij}, γ, σ are the conservative, dissipative and random coefficients, respectively, r_{ij} is the distance with the corresponding unit vector $\hat{\mathbf{r}}_{ij}$, $\hat{\mathbf{v}}_{ij}$ is the difference between the two velocities, ζ_{ij} is a Gaussian random number with zero mean and unit variance, and dt is the simulation timestep size. The parameters γ and σ and the weight functions coupled through the fluctuation-dissipation theorem and are related by $\omega_d = \omega_r^2$ and $\sigma^2 = 2\gamma k_B T$, where k_B is the Boltzmann constant and T is the temperature of the system. The weight function $\omega_r(r_{ij}) = (1-r_{ij}/r_c)^k$ with $k = 1$ in the standard DPD method, whereas other values of k have been used to increase the fluid viscosity (3). More detailed description of DPD method can be found elsewhere (4, 5); see also (6) for RBC and platelet modeling.

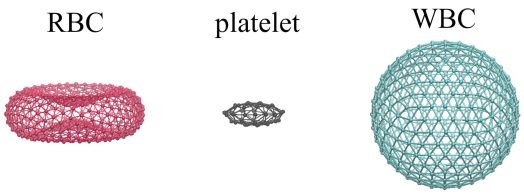

Figure S1: Schematic of the RBC, platelet, and WBC models.

In addition to blood plasma modeled by collections of free DPD particles, the membrane of suspending cells including RBCs, platelets, and WBCs is constructed by a 2D triangulated network with N_v vertices (DPD particles). The vertices are connected by N_s elastic bonds to impose proper membrane mechanics, see the schematic cell models in Fig. S1. This DPD representation of RBCs, platelets, and WBCs was extensively used and validated in the previous studies for both healthy and diseased cells (6–9). For a single cell, the free energy (V_{cell}) is given by

$$V_{cell} = V_s + V_b + V_{a+v}. \tag{5}$$

The elastic energy V_s representing the elastic interactions of the cell membrane is defined by

$$V_s = \sum_{j \in 1 \dots N_s} \left[\frac{k_{\mathrm{B}} T l_m (3x_j^2 - 2x_j^3)}{4p(1 - x_j)} + \frac{k_p}{l_j} \right], \tag{6}$$

where p is the persistence length, k_p is the spring constant, $k_{\mathrm{B}}T$ is the energy unit, l_j is the length of the spring j, l_m is the maximum spring extension, and $x_j = l_j/l_m$. p and k_p are computed by balancing the forces at equilibrium and from their relation to the macroscopic shear modulus, μ_s:

$$\mu_s = \frac{\sqrt{3} k_{\mathrm{B}} T}{4 p l_m x_0} \left(\frac{x_0}{2(1 - x_0)^3} - \frac{1}{4(1 - x_0)^2} + \frac{1}{4} \right) + \frac{3\sqrt{3} k_p}{4 l_0^3}, \tag{7}$$

where l_0 is the equilibrium spring length and $x_0 = l_0/l_m$. The bending resistance V_b of the cell membrane is modeled by

$$V_b = \sum_{j \in 1 \dots N_s} k_b \left[1 - cos(\theta_j - \theta_0) \right], \tag{8}$$

where k_b is the bending constant, and it is related to the macroscopic bending rigidity k_c with the expression $k_b = 2k_c/\sqrt{3}$, θ_j is the instantaneous angle between two adjacent triangles having the common edge j, and θ_0 is the spontaneous angle. In addition, the area and volume constraints V_{a+v} are imposed to mimic the area-preserving lipid bilayer and the incompressible interior fluid. The corresponding energy is given by

$$V_{a+v} = \sum_{j \in 1 \dots N_t} \frac{k_d (A_j - A_0)^2}{2A_0} + \frac{k_a (A_{\text{cell}} - A_0^{\text{tot}})^2}{2A_0^{\text{tot}}} + \frac{k_v (V_{\text{cell}} - V_0^{\text{tot}})^2}{2V_0^{\text{tot}}}, \tag{9}$$

where N_t is the number of triangles in the membrane network, A_0 is the equilibrium value of a triangle area, and k_d, k_a and k_v are the local area, global area and volume constraint coefficients, respectively. The terms A_0^{tot} and V_0^{tot} are targeted cell area and volume. In practice, we use high values for the constraint coefficients to enforce area and volume incompressibility.

Fluid-cell interactions are achieved through viscous friction using the dissipative and random DPD forces. In order to impose appropriate boundary conditions between the fluid and the cell membrane, a DPD dissipative force ($\mathbf{F}^D$) between fluid particles and membrane vertices needs to be properly applied. The dissipative coefficient γ is computed such that no-slip condition on cell surface is enforced and γ is derived based on the idealized case of linear shear flow over a patch of RBC membrane. The total shear force exerted by the fluid on a patch of area A is equal to $A\eta\dot{\gamma}$, where η is the viscosity of fluid and $\dot{\gamma}$ is the local wall shear rate.

In DPD discrete form, we distribute a number of particles on the wall to mimic the membrane vertices. The force (F_v) on a single wall particle exerted by the fluid can be found as follows

$$F_v = \int_{V_H} ng(r)\mathbf{F}^D \mathrm{d}V\,, \tag{10}$$

where n is the fluid number density, $g(r)$ is the radial distribution function of fluid particles with respect to the wall particles, and V_H is the half sphere volume of fluid above the wall. The total shear force on the area A is equal to $F_v N_A$, where N_A is the number of wall particles on the patch with area A. The radial distribution function is uniform $g(r) = 1$ when the repulsive conservative interaction between fluid and wall particles is zero (6, 10). The repulsive-force coefficient for the fluid-cell interactions is therefore set to zero, and the dissipative coefficients can be computed through the equality of $F_v N_A = A\eta\dot{\gamma}$. The DPD parameters used in eqn (2)-(4) for all types of DPD particles and the cell membrane parameters used in eqn (6)-(9) for all blood cell models are given in Tables S1 and S2, respectively.

Table S1: DPD parameters used in simulations. r_c is the cut-off radius, a_{ij} is the conservative coefficient, γ is the dissipative coefficient, and k is the weight function exponent. In all simulations, we set the particle mass $m = 1$, and the thermal energy $k_B T = 0.10$ in DPD units. Note that S= solvent (representing plasma), R= RBC, P= platelet, and W= WBC.

type	r_c	a_{ij}	γ	k
S-S	1.58	5.0	20.0	0.20
S-R	1.5	0.0	45.0	0.20
S-P/S-W	1.5	0.0	10.0	0.20
R-R	1.0	10.0	10.0	0.20
R-P/R-W	1.0	10.0	10.0	0.20
P-P/P-W/W-W	1.0	10.0	10.0	0.20

In order to prevent cell overlap we also adopt a Morse potential between cell membrane particles in the form of

$$V_M(r) = D_e[e^{2\beta(r_0-r)} - 2e^{\beta(r_0-r)}]\,, \tag{11}$$

where r is the separation distance, r_0 is the zero force distance, D_e is the well depth of the potential, and β characterizes the interaction range. By properly setting the parameters, we can ensure strong repulsive forces between cell membrane particles and prevent their overlap. We present the Morse potential parameters used for cell-cell interactions in Table S3. Note that the cutoff radius $r_{cM} = 1$ is set for all the Morse interactions.

It is also important to derive the scaling relationships between model (DPD) units and physical units. We first define the length scale as

$$r^M = \frac{D_0^P}{D_0^M}\,, \tag{12}$$

where D_0 is the RBC diameter, r^M is the model unit of length, and the superscripts M and P denote the model and physical units, respectively. In the current study, we consider D_0^P = 7.82$\times 10^{-6}$ m (11), D_0^M = 7.82, then r^M = 1.0$\times 10^{-6}$ m can be obtained. In addition, the time scale is defined as

$$\tau = \frac{D_0^P}{D_0^M}\frac{\eta^P}{\eta^M}\frac{\mu_0^M}{\mu_0^P}\,, \tag{13}$$

Table S2: Cell membrane parameters for normal RBCs (NRBCs), diabetic RBCs (DRBCs), platelets with mean platelet volume (MPV)= 6 fL (PLTs), platelets with MPV= 12 fL (PLT*), and white blood cells (WBCs). N_v is the number of DPD particles on the membrane, l_m is the maximum bond extension, l_0 is the equilibrium bond length, k_b is the bending constant, μ_s is the shear modulus, A_0^{tot} and V_0^{tot} are the specified cell area and volume, respectively, $k_d + k_a$ is the combined area constraint coefficient, and k_v is the volume constraint coefficient.

cell	N_v	l_m/l_0	k_b	μ_s	A_0^{tot} (V_0^{tot})	$k_d + k_a$ (k_v)
NRBC	500	1.8	6.025	100.0	132.87 (92.45)	5000 (5000)
DRBC	500	1.8	6.025	200.0	132.87 (127.45)	5000 (5000)
PLT	48	1.8	100.0	10^4	19.63 (6.02)	5000 (10^4)
PLT*	48	1.8	100.0	10^4	31.16 (12.01)	5000 (10^4)
WBC	2498	1.8	6.025	2200.0	313.78 (522.44)	50000 (5×10^4)

Table S3: Morse potential parameters for cell-cell interactions. D_e is the well depth of the potential, r_0 is the zero force distance, and β characterizes the interaction range. Note that R= RBC, P= platelet, and W= WBC.

type	D_e	β	r_0
R-R	5.0	2.0	0.95
R-P/R-W	10.0	2.0	1.0
P-P/P-W/W-W	10.0	2.0	1.0

where η is the viscosity of plasma and μ_0 is the RBC shear modulus. In this study, we consider η^P = 1.25×10^{-3} Pa·s, μ_0^P = 4.73×10^{-6} N/m, η^M= 148 and μ_0^M = 100 (6, 12, 13), then the DPD time scale is τ = 1.8×10^{-4} s. The size of a DPD particle for representing blood plasma can be estimated by

$$V_{dpd} = V_D/N_l\,, \tag{14}$$

where we used the volume of the modeled domain V_D = 113411.5 μm^3 and the number of solvent particles in the domain N_l= 365014. Hence, a particle size is V_{dpd} = 3.1×10^{-19} m^3. The volume of a water molecule is $\sim3\times10^{-29}$ m^3 (14). Therefore, the mapping between the water molecules and a solvent bead in our system is at the scale of $\mathcal{O}(10^{10})$ water molecules/DPD particle.

Appendix B. DPD model validation

The focus of this study is quantifying platelet margination in diabetic blood flow via a high-fidelity numerical approach. It is important to validate the numerical model prior to using it in applications extensively. As there is little to no available microfluidic data on platelet margination in the literature, we resort to the measurements made for marginated polystyrene micro-beads suspended in bovine blood from the work of Carboni *et al.* (15).

In order to have the closest possible comparison with the experimental measurements, a rectangular channel with the same height ($40\ \mu m$) is considered in our DPD simulations with human blood driven by the pressure gradient, which generates different flowrates corresponding to wall shear rates of 60 and 120 s^{-1} similar to the experiment. The width of the channel is assumed to be much larger than its height, which makes

the DPD system periodic along the width of the channel. Further, we assume a periodic channel flow along the flow direction. Rigid spherical particles of variable sizes, 0.53, 0.84 and 2.11 μm, are modeled by DPD particles connected to each other through stiff wormlike chains (WLCs) (16) similar to the model described for platelets. For smaller beads, however, 12 DPD particles are used to form the sphere, as opposed to 42 DPD particles used for the largest bead.

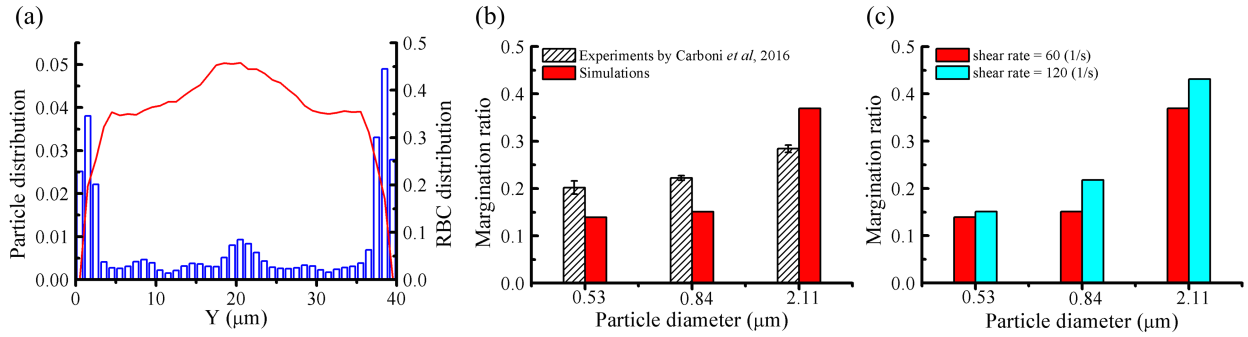

Figure S2: DPD model validation and comparison with microfluidic measurements for rigid spherical particles. (a) Time-averaged particle (bars) and RBC volume fraction (red line) along the channel height (particle diameter 2.11 μm). (b) Comparison of computed and measured margination ratios for spherical particles of different sizes, with experimental data by Carboni *et al.* (15). (c) Computed margination ratios for different particle sizes evaluated for two wall shear rates.

A representative result for time-averaged particle and RBC distributions across the channel height is given in Fig. S2, where both distributions are given as volume fractions. The mean volume fraction of RBCs is 35% (blood hematocrit used in experiments (15)), a rise in RBC volume fraction close to the center of the channel and the depletion of RBCs adjacent to the channel walls are clear. The cell free layer (CFL) thickness is estimated to be $\approx 2\mu m$, which is used for calculating the margination ratio. The spherical particles volume fraction is quite higher in the CFL due to the margination effects.

Margination ratio (referred to as *margination percentage* in the main text) defined as the ratio of marginated particles in the CFL divided by the number of suspended particles is plotted in Fig. S2(b) for three different particle sizes at wall shear rate 60 s^{-1}. The results show good comparison with the experiments, suggesting that the margination ratio increases by the size of the particles. The difference, however, could be attributed to the image resolution in the experiments and the fact that bin sizes considered in the experiment are relatively larger than the CFL thickness. It is also noted that the different sizes of RBCs adopted in the experiment (15) and simulation (bovine RBCs with diameter 5-6 μm (17) vs. human RBCs with diameter 7.5-8.7 μm (11)) could lead to slight differences in the magnitude of margination ratio in our simulations. However, the simulation results will not be affected qualitatively because we keep the blood hematocrit (H_{ct}= 35%) the same as the experiments (15). The volume fraction of RBCs is detrimental in the frequency of particle collisions with the RBCs that leads to particle margination (18, 19). In addition, the effect of shear rate on particles margination is plotted in Fig. S2(c). Increasing the shear rate enhances particle margination (which is observed for oblate platelets as well) for all particle sizes as reported by the experiment of Carboni *et al.* (15), and confirmed in a few other numerical simulations (6, 20). In the current model validation, we only consider particles with spherical shapes and not the oblate spheroids (the shape of a resting platelet) since spherical polystyrene micro-beads were used in the experiment. In fact, particle shapes are also important for margination, which have been investigated numerically in a few other studies. Reasor *et al.* (21) observed that comparing with the spherical particles, the oblate particles (in particular the disk-like oblates) were easily trapped in the center-occupied RBC core, lowering their margination rate. On the other hand, Vahidkhah and Bagchi (22) found that the frequency of particle-RBC collision played a key role in determining particle margination rate, and the oblate particles of moderate aspect ratio (AR=0.5) exhibited the highest frequency among the spherical, rod-like, and oblate particles (AR=0.3,0.5).

Appendix C. Blood sample preparation and analysis procedures

Clinical data from 136 consecutively subjects were pulled from the biochemical database of the S. Lepida Biomedical Laboratory in Athens Greece specifically for this study. Data had been obtained using standard automatic biochemical analyzers (Sysmex XT-1800i and ILAB 350 Clinical Chemistry System) were anonymized and thus exempt from IRB oversight. Clinical data included HbA1c, fasting glucose level, mean corpuscular volume (MCV), mean platelet volume (MPV), plateletcrit (PCT), and WBC counts. A total of 64 type 2 diabetic patients (30 males and 34 females; age, 61$\pm$13.69 years; range, 34 – 90 years) and 72 healthy controls (30 males and 42 females; age, 52$\pm$17.80 years; range, 26 – 94 years) were included in the study, and the clinical data were analyzed by one-way analysis of variance (ANOVA). Variables given as absolute or mean value $\pm$ standard error are shown in Table S4. Statistical significance was defined as $p <$0.05.

As shown in Table S4 and Fig. S3, despite the slightly decreased mean value of MCV in diabetic subjects, $p =$0.05 estimated based on one-way ANOVA test indicates no significant difference in MCV of control and diabetic blood samples. On the other hand, there are significantly higher MPV (10.0$\pm$1.26 fL vs 9.2$\pm$1.70 fL, $p =$0.003), PCT (0.23$\pm$0.06 % vs 0.21$\pm$0.07 %, $p =$0.02), and WBC count (8.04$\pm$2.16 k/μL vs 6.85$\pm$1.96 k/μL, $p =$0.001) for diabetic subjects compared with non-diabetics.

Table S4: Clinical characteristics of the study groups

	Controls	Diabetics	p-value
Total subject number	72	64	–
Male/ Female	30/ 42	30/ 34	–
Age range (years)	26 – 94	34 – 90	–
Mean age (years)	52 $\pm$ 17.80	61 $\pm$ 13.69	–
Mean HbA1c (%)	5.25 $\pm$ 0.29	7.66 $\pm$ 1.41	–
Fasting glucose (mg/dl)	99.0 $\pm$ 15.4	144.5 $\pm$ 45.8	–
MCV (fL)	88.33 $\pm$ 7.76	85.26 $\pm$ 9.89	0.05
MPV (fL)	9.2 $\pm$ 1.70	10.0 $\pm$ 1.26	0.003
PCT (%)	0.21 $\pm$ 0.07	0.23 $\pm$ 0.06	0.02
WBC count (k/μL)	6.85 $\pm$ 1.96	8.04 $\pm$ 2.16	0.001

Variables are expressed as mean value $\pm$ standard error. Note that MCV= mean corpuscular volume, MPV= mean platelet volume, and PCT= plateletcrit. p-value is estimated based on one-way ANOVA test.

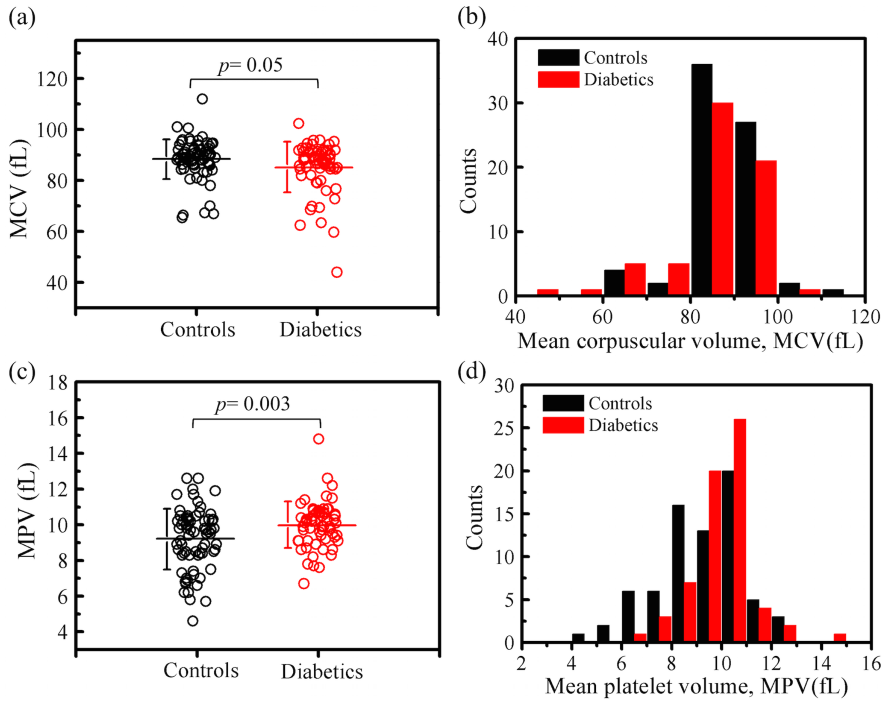

Figure S3: Mean corpuscular volume (MCV) and mean platelet volume (MPV) from healthy controls and diabetic patients. (a) and (c) Scatter plots of all measured data, where the horizontal lines are mean values and the vertical error bars are the sample standard deviation. (b) and (d) Histograms showing the count distributions of MCV and MPV in controls and diabetics.

References

1. Fedosov, D. A., W. Pan, B. Caswell, G. Gompper, and G. E. Karniadakis, 2011. Predicting human blood viscosity in silico. *Proc. Natl. Acad. Sci. U.S.A* 108:11772–11777.

2. Ye, T., N. Phan-Thien, and C. T. Lim, 2016. Particle-based simulations of red blood cells - a review. *J. Biomech.* 49:2255–2266.

3. Fan, X., N. Phan-Thien, S. Chen, X. Wu, and T. Yong Ng, 2006. Simulating flow of DNA suspension using dissipative particle dynamics. *Phys. Fluids* 18:063102.

4. Espanol, P., and P. Warren, 1995. Statistical mechanics of dissipative particle dynamics. *Europhys. Lett.* 30:191.

5. Groot, R. D., and P. B. Warren, 1997. Dissipative particle dynamics: bridging the gap between atomistic and mesoscopic simulation. *J. Chem. Phys.* 107:4423–4435.

6. Yazdani, A., and G. E. Karniadakis, 2016. Sub-cellular modeling of platelet transport in blood flow through microchannels with constriction. *Soft Matter* 12:4339–4351.

7. Fedosov, D. A., B. Caswell, and G. E. Karniadakis, 2010. A multiscale red blood cell model with accurate mechanics, rheology, and dynamics. *Biophys. J.* 98:2215–2225.

8. Pivkin, I. V., and G. E. Karniadakis, 2008. Accurate coarse-grained modeling of red blood cells. *Phys. Rev. Lett.* 101:118105.

9. Lei, H., and G. E. Karniadakis, 2013. Probing vasoocclusion phenomena in sickle cell anemia via mesoscopic simulations. *Proc. Natl. Acad. Sci. U.S.A* 110:11326–11330.

10. Fedosov, D. A., B. Caswell, A. S. Popel, and G. E. Karniadakis, 2010. Blood flow and cell-free layer in microvessels. *Microcirculation* 17:615–628.

11. Diez-Silva, M., M. Dao, J. Han, C.-T. Lim, and S. Suresh, 2010. Shape and biomechanical characteristics of human red blood cells in health and disease. *MRS Bulletin* 35:382–388.

12. Baskurt, O. K., M. R. Hardeman, and M. W. Rampling, 2007. Handbook of hemorheology and hemodynamics, volume 69. IOS press.

13. Hochmuth, R. M., and R. E. Waugh, 1987. Erythrocyte membrane elasticity and viscosity. *Annu. Rev. Physiol.* 49:209–219.

14. Chang, H.-Y., Y.-L. Lin, Y.-J. Sheng, and H.-K. Tsao, 2012. Multilayered polymersome formed by amphiphilic asymmetric macromolecular brushes. *Macromolecules* 45:4778–4789.

15. Carboni, E. J., B. H. Bognet, G. M. Bouchillon, A. L. Kadilak, L. M. Shor, M. D. Ward, and A. W. Ma, 2016. Direct tracking of particles and quantification of margination in blood flow. *Biophys. J.* 111:1487–1495.

16. Marko, J. F., and E. D. Siggia, 1995. Stretching DNA. *Macromolecules* 28:8759–8770.

17. Adili, N., M. Melizi, H. Belabbas, and A. Achouri, 2014. Preliminary study of the influence of red blood cells size on the determinism of the breed in cattle. *Vet. Med. Int.* 2014:429495.

18. Kumar, A., and M. D. Graham, 2012. Margination and segregation in confined flows of blood and other multicomponent suspensions. *Soft Matter* 8:10536–10548.

19. Kumar, A., R. G. H. Rivera, and M. D. Graham, 2014. Flow-induced segregation in confined multicomponent suspensions: effects of particle size and rigidity. *J. Fluid Mech.* 738:423–462.

20. Mehrabadi, M., D. N. Ku, and C. K. Aidun, 2016. Effects of shear rate, confinement, and particle parameters on margination in blood flow. *Phys. Rev. E* 93:023109.

21. Reasor, D. A., M. Mehrabadi, D. N. Ku, and C. K. Aidun, 2013. Determination of critical parameters in platelet margination. *Ann. Biomed. Eng.* 41:238–249.

22. Vahidkhah, K., and P. Bagchi, 2015. Microparticle shape effects on margination, near-wall dynamics and adhesion in a three-dimensional simulation of red blood cell suspension. *Soft Matter* 11:2097–2109.